EFFECTS OF AL^{3+}, PR^{3+} AND MN^{2+} SUBSTİTUTİON ON THE STRUCTURAL AND DİELECTRİC PROPERTİES OF M-TYPE BARİUM HEXAFERRİTES

Y. ABDU[1] & I. M. MUSA[2]
[1]Department of Physics, Bayero University, Kano. Nigeria.
[2]Department of Physics, Federal University Dutse, Jigawa State. Nigeria.
Email: yunusa_abdu@yahoo.com, ayunusa.phy@buk.edu.ng
Phone No: +234-802-917-4511

Abstract

Metal-type (M-type) barium hexaferrites are an important microwave absorbing materials. However, research studies have shown that microwave absorbing ability of M-type hexaferrites is strongly dependent on the method of synthesis and doping with cations in the parent material. The method of synthesis and doping form the mechanism for substitution of foreign ions into Ba^{2+}*,or* Fe^{3+} *sites. Although, previous studies revealed that substitution of transition rare earth elements and post transition metal ions has led to a large change in the electromagnetic properties of the hexaferrites, this change gives the material high microwave absorbing capacity. This change is accompanied with some drawbacks which include non-coverage of all frequency range that is mainly associated with the synthesis technique and doping procedure. This work presents dielectric property enhancement of the M-type hexaferrites by introducing more than one dopant using sol-gel autocombustion technique. M-type Barium hexaferrites with* $Ba_{0.8-x}Ca_{0.2}Al_xFe_{12-2y}Pr_yMn_yO_{19}$ *(x= 0.00, 0.04, 0.08 y= 0.00, 0.06, 0.09) chemical compositions was successessfully synthesized via sol-gel auto-combustion technique. The formation of single phase hexagonal ferrites was confirmed from XRD peaks. The presence of hematite as an inpurity was observed in the doped sample, the cystallites sizes were in the range 20.5–26.33 nm. The lattice constants were found to decrease with increase in ion substitution. The FTIR spectra of the sample show three dominant peaks in the range 400-600* cm^{-1} *which indicate the formation of the desired hexaferrites structure. The dielectric properties typical of hexaferrites with low dielectric loss was confirmed on all the samples. The dielectric constant was enhanced at high frequency in the entire sample and reduction of dielectric loss was also observed which was dependent on ion substitution. The grain boundary resistance contributes most to the dielectric properties as indicated by the Nyquist plot, whereas the AC conductivity is the dominant conducting mechanism in the material which was found to decrease with increase in ion substitution. The properties of the synthesized material could be useful for applications in electronic and high frequency absorbing devices.*

Keywords: M-type nano-hexaferrites, sol-gel auto-combustion, metal ions substitutions, materials properties

Introductıon

The rapid development of electronic devices operating at microwave frequency range has resulted in the increasing problems of electromagnetic interference (EMI). However, M-type hexaferrites with remarkable magnetic and Dielectric properties have been known to serve as important microwave absorbing materials (Pullar, 2012; Mohammed, *et, al*; 2019; Tchouank Tekou, *et, al,* 2019; Bhat & Want, 2016). The resistivity of m-type hexaferrites is very high as a result of this, the dominant absorbing mechanism is magnetic loss. Hence, an improvement in the intrinsic magnetic properties such as saturation magnetization and magneto-crystalline anisotropy or coercivity is needed to enhance their microwave absorbing ability (Bhat & Want, 2016, Hafeez, *et, al;* 2019, Sharma, *et, al;* 2017, Mohammed, *et, al*; 2017). Recent researche studies have shown that microwave absorbing ability of M- type Hexaferrites are strongly dependent on the method of synthesis and doping with cations in the parent material. That is the Magnetic and microwave properties can be modulated by foreign ions substitutions to Ba^{2+} or Fe^{3+} sites (Chawla*, et, al*; 2015, Ndikilar*, et, al*; 2019 and Mohammed*, et, al*; 2018). It was reported by various researchers that the substitutions of transition, rare earth elements (RE) and post transition metal ions lead to the large change in the electromagnetic properties of ferrites which allow for ferrites to have high microwave absorbing capacity. For example, the substitution of Gd-Co, Cr-Zn and Ca leads to reduction in HA also the substitution of Sc or In for Fe reduces HA allowing for applications from X-, Ku-, K-, to Ka-bands (Mosleh, *et, al*; 2016, Sun, *et, al*; 2012 , Pullar & Bhattacharya, 2001, Rafiq, *et al*; 2017 & Vadivelan & Victor, 2016). While substitution of Al and Ga leads to increases in HA and device operation at frequencies up to U-, E-, and W-bands. In essence, the BaM hexaferrite, and its substitutional systems, allow for device applications from 1 to 100 GHz. The major drawbacks of these materials are the non-coverage of all frequency range attributed to the inability to decrease the coercivity and simultaneously increase the saturation magnetization which is mainly associated with the syntheses technique and doping procedure.

In this research work, an attempt is made to improve and enhance the dielectric properties of M-type hexaferrites by introducing more than one dopant using sol-gel auto-combustion techniques. It was aimed at enhancing the Electromagnetic properties of hexaferrite by the substitutions of various cations in Ba^{2+}, Fe^{3+} and Fe^{2+}sites.

Materials and synthesis

The synthesis of the required hexaferrite was done using chemicals obtained from LOBA Chemie which include ferric nitrate ($Fe(NO_3)_3.9H_2O$), barium nitrate ($Ba(NO_3)_2$), calcium nitrate $Ca(NO_3)_2.4H_2O$ Aluminum nitrate $Al(NO_3)_3.9H_2O$, manganese nitrate ($Mn(NO_3)_2.H_2O$, praseodymium nitrate $Pr(NO_3)_3.6H_2O$, and citric acid ($C_6H_8O_7$). These chemicals were used in order to prepare $Ba_{0.8-x}Ca_{0.2}Al_xFe_{12-2y}Pr_yMn_yO_{19}$ (x= 0.00, 0.04, 0.08 y= 0.00, 0.06, 0.09) BaM via sol-gel auto-combustion techniques. The required amounts of the metal salt were weighed in stoichiometric ratios and dissolved in ethylene glycol to form the salt solution, maintaining the molar ratio of citric acid to metal nitrates at 1:1.5. To adjust the pH to 7.00 ammonia solution was added dropwise. The solution was heated with a magnetic heating stirrer at 80-100 ^oC for 3 hours which evaporated the ethylene glycol and obtained the gel viscous solution. The solution was then heated at 280-300 ^oC for about 30 minutes which resulted in the gel turning into fluffy precursor powder. This process was accompanied by auto-combustion and emission of volatile gases of HNCO, NH_3, and N_2. The precursor materials were calcinated at 1100 ^oC for 6 hours to obtain the desired hexagonal phase. The chemical composition and their assigned codes are shown in table 1.

Table 1: Sample code of Al^{3+}, -Pr^{3+}, -Mn^{2+} substituted nanoparticles

Sample code	x	y	Sample Composition
MA1	0	0	$Ba_{0.8}Ca_{0.2}Fe_{12}O_{19}$
MA2	0.04	0.06	$Ba_{0.76}Ca_{0.2}Al_{x0.04}Fe_{11.88}Pr_{0.06}Mn_{0.06}O_{19}$
MA3	0.08	0.09	$Ba_{0.72}Ca_{0.2}Al_{0.08}Fe_{11.82}Pr_{0,09}Mn_{0.09}O_{19}$

Characterization Techniques

The x-ray diffractometer (XRD) (Bruker AXSD8 advance diffractometer) was used to study the structure of the synthesized M-type hexaferrites. XRD patterns were recorded between 20°–80° range. Fourier transform infrared (FTIR) spectrometer (Nicolet FTIR interferometer IR prestige-21 (model-8400S)) was used to study the nature of the attached functional groups of the material. The study of the morphology of the samples was done using FESEM, MIRA3 TESCAN, USA instrument. The FESEM was operated at 5 mm working distance with 5 to 10 kV accelerating voltage.

Impedance analyzer (Wayne Kerr 6500B) having 0 to +40V DC bias voltage and 0 to 100 mA DC bias Current was used in calculating all dielectric parameters (dielectric constant, dissipation factor and AC conductivity). However, the impedance spectra were recorded via passing radiation through a 9 mm thickness pellet prepared by coating with silver conducting paint, to make them suitable for use in the measuring instrument.

Results and Dıscussıon

XRD Analysis

The XRD spectra of $Ba_{0.8-x}Ca_{0.2}Al_xFe_{12-2y}Pr_yMn_yO_{19}$ (x= 0.00, 0.04, 0.08 y= 0.00, 0.06, 0.09) are shown in Fig. 1. The diffraction peaks were indexed using JCPDS card no. 39–1433. The XRD peaks (all the peak reflections) confirm the formation of pure M-type magnetoplumbhite structure hexagonal structure. The XRD spectra also reveal an absence of impurities in the undoped sample (MA1) with presence of hematite as an impurity in the doped sample (MA3). It was also observed from Fig. 1 that there is slight shift of XRD peaks towards high diffraction angles after doping. Table 1. Shows the calculated crystallite size of the samples using Scherer’s formula

$$D = \frac{k\lambda}{\beta cos\theta} \qquad (1)$$

where D is the crystal size, k is the shape factor = 0.9, β is the line broadening at half the maximum intensity (FWHM) in radians, λ=1.5406Å is the X-ray source of radiation wavelength and θ is the Bragg's diffraction angle. The crystallite size decreases with increasing in substitution of small ionic radii. This occur as a result of the strain produced in the unit cell and the inhibition behaviour of rare earth elements in magneto-plumbhite. Moreover the crystallite size reduction causes broadening of characteristic peaks of the full width at half maxima (Tchouank Tekou, et, al; 2019, Bhat and Want, 2016, Hafeez, et, al; 2019 & Sharma, *et, al*; 2017).

Equation 2.0 was used to obtained lattice parameters a and c of all the samples

$$\frac{1}{d_{hkl}^2} = \frac{4}{3}\left(\frac{h^2+hk+k^2}{a^2}\right) + \frac{l^2}{c^2} \qquad (2)$$

where d_{hkl} is a crystal face distance and h, k, l are miller indices. The values of lattice parameters for all the samples are shown in Table 1. These values slightly decreases with the substitution of the elements. The increase in concentration of the dopants prompted the reduction in a and c-axis. The volume of unit cell (Vcell) is given as:

$$V_c = 0.8666a^2c \qquad (3)$$

Due to the dependency of Vc on the lattice parameters, the same behaviour was observed in the variation of Vc with substitution. This behaviour would be attributed to an interaction between substituted cations and microstructural defects (Mohammed, *et ,al*; 2017 & Tchouank Tekou, *et al*; 2017). The distance between magnetic ions determine the Variation in lattice parameter (a and c) which causes change of exchange in the interaction and leads to variation in the magnetic properties (Chawla, *et, al*; 2015, Ndikilar, *et, al*; 2019 & Mohammed, *et, al*; 2018). With this we can conclude that the increase in substitution causes the changes in easy magnetization of c-axis to be greater than that of a-axis. Furthermore, it was observed that the c/a ratio is not greater than 3.98 as shown in table 2., therefore all the samples exhibits hexagonal structure, due to the fact that the hexagonal ferrite material’s c/a ration must not be greater than 3.98 for it to have hexagonal structure

[(Tchouank Tekou, *et al*; 2017, Chawla, *et, al*; 2015 & Ndikilar, *et, al*; 2019). The average values of the crystallites size are shown in table 1. These was found to be in the range 20.50–26.33nm. The average crystallite size for MA1, MA2 and MA3 are 26.33, 20.95, and 20.50nm, respectively. Sample MA1 with average crystallite size of 26.33nm was observed to be the maximum size obtained.

Table 2: Calculated Structural parameters from XRD result

Sample	2theta	d(A)	beta	A	c	V	c/a	D	η	ε
MA1	30.202	2.95675	0.309	5.9135	23.28064	705.5094	3.936863	263.3267	-0.00479	0.000728
MA2	30.326	2.94491	0.263	5.88982	23.21936	698.0282	3.942287	209.4744	-0.00404	0.000622
MA3	30.368	2.94102	0.397	5.88204	23.1892	695.2811	3.942374	205.0374	-0.00608	0.00094

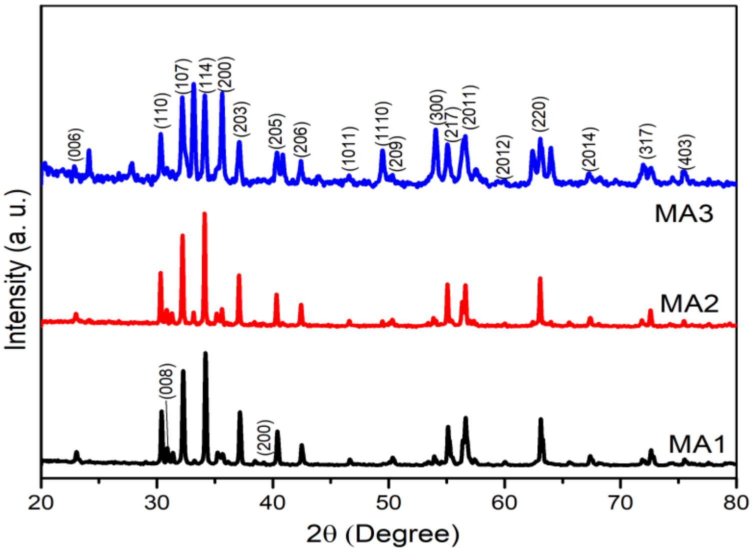

Fig. 1: XRD spectra of $Ba_{0.8-x}Ca_{0.2}Al_xFe_{12-2y}Pr_yMn_yO_{19}$ (x= 0.00, 0.04, 0.08 y= 0.00, 0.06, 0.09)

FTIR Results

The FTIR spectra $Ba_{0.8-x}Ca_{0.2}Al_xFe_{12-2y}Pr_yMn_yO_{19}$ (x= 0.00, 0.04, 0.08 y= 0.00, 0.06, 0.09) is shown in Figure 1b. The characteristics bands were observed on each spectrum in the range of 400-600 cm^{-1}, specifically at 574 cm^{-1},541 cm^{-1} and 418cm^{-1}. These prominant peaks correspond to a symmetric stretching and out plane vibrations of metal oxide (Fe-O) in octahedral and tetrahedral sites and give an idea of the formation of hexaferrites. The peak at 894 cm^{-1} is related to O-Fe-O vibration mode. The small band around 1530 cm^{-1} reveals the vibration of metal oxygen metal (M-O-M) bond, which is represented by iron-oxygen-iron. The intense facinating bands aroun 2060cm^{-1} and 2375 cm^{-1} could be assigned to the O-C-O stretching bands (Mohammed, et, al; 2018). The peak at 3737 cm^{-1} corresponds to the vibration of the hydroxyl group in the sample which is attributed to bending mode of H-O-H.

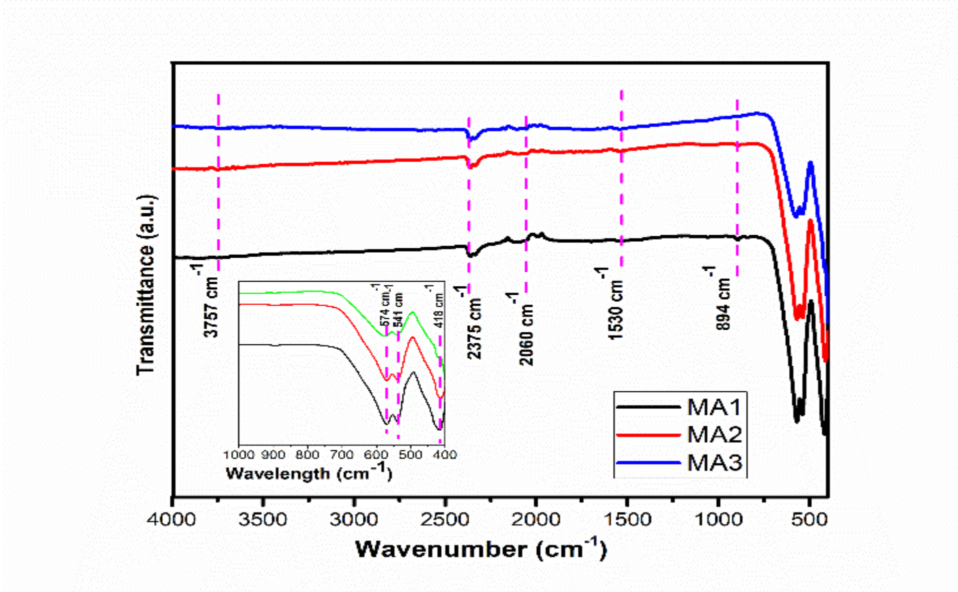

Figure 2: The FTIR spectra $Ba_{0.8-x}Ca_{0.2}Al_xFe_{12-2y}Pr_yMn_yO_{19}$ (x= 0.00, 0.04, 0.08 y= 0.00, 0.06, 0.09)

FESEM Results

FESEM micrographs of $Ba_{0.8-x}Ca_{0.2}Al_xFe_{12-2y}Pr_yMn_yO_{19}$ hexaferrites with Al^{3+}-Pr^{3+}-Mn^{2+} content (x and y) of x=0, y=0 and x=0.04, y=0.06 are shown in figure 3a and 3c respectively. The micrographs show that the sample exhibits hexagonal platelet-like structure (morphology) and the average grain size changes with the introduction of the dopant as seen in figure 3b and d. The average crystalline size observed from FESEM micrographs are 22.76 nm and 25.85 nm, respectively. There also exist a magnetic interaction between the particles which causes agglomeration and non uniform distribution of the grains.

The EDX spectra and the elemental mapping images of $Ba_{0.8-x}Ca_{0.2}Al_xFe_{12-2y}Pr_yMn_yO_{19}$ show the existence of Ca, Ba, Fe and O for the sample with of x=0, y=0 and Ca, Mn, Ba, Fe, Pr, Al and O for Sample with x=0.04, y=0.06. This confirm the formation of the desired composition, as presented in Figure 4a and 4b.

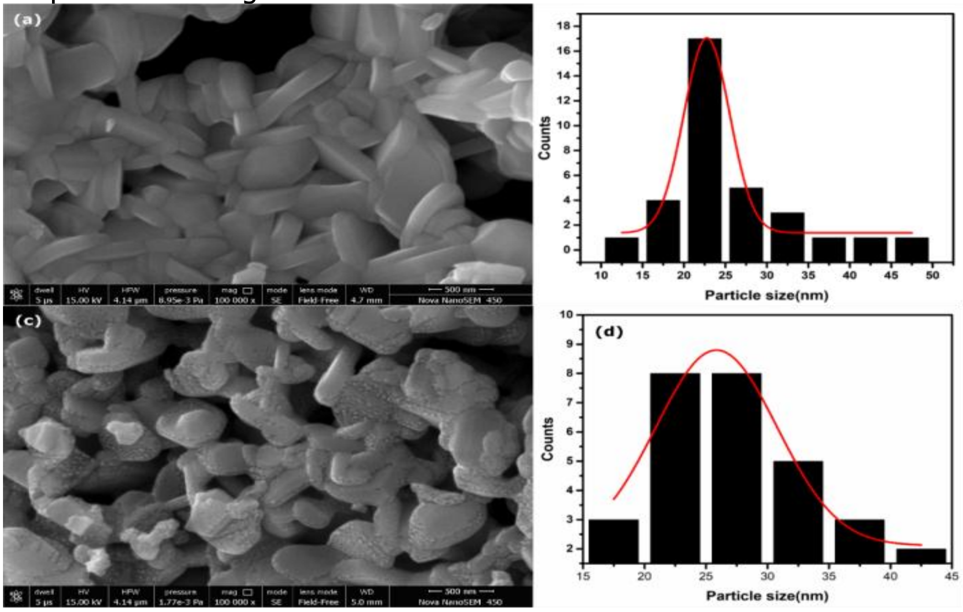

Figure 3: FESEM micrographs of $Ba_{0.8-x}Ca_{0.2}Al_xFe_{12-2y}Pr_yMn_yO_{19}$

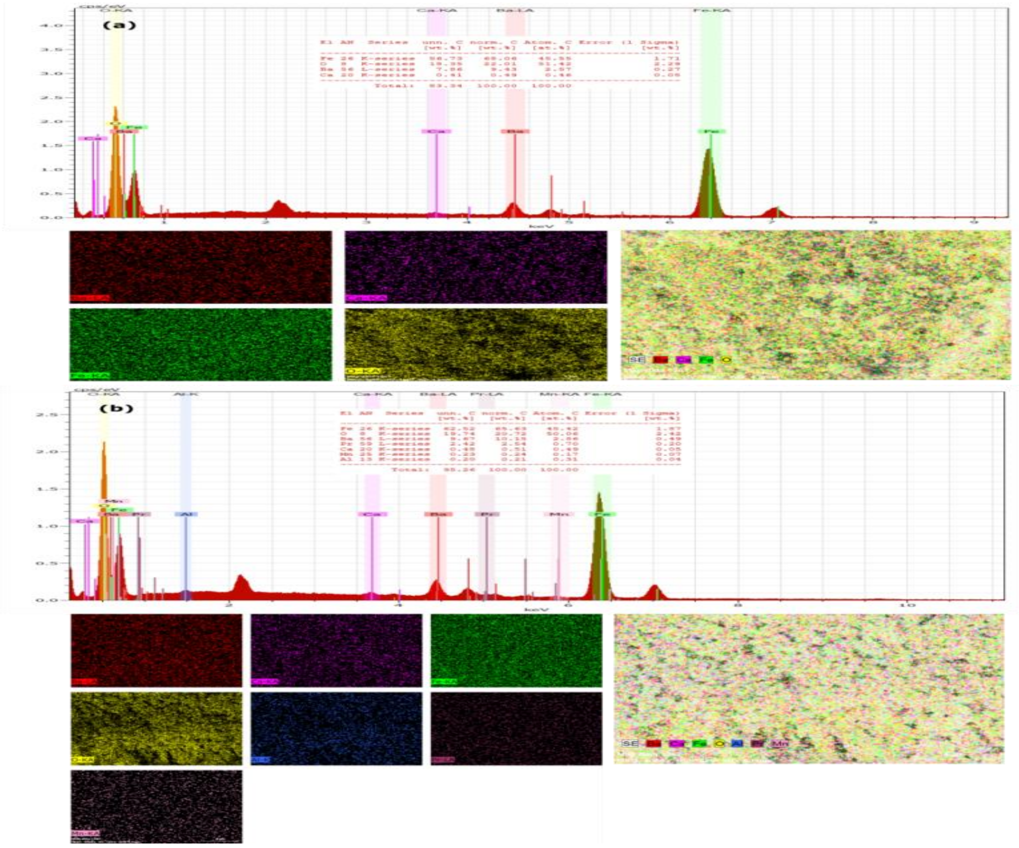

Figure 4: EDX and Mappıng of $Ba_{0.8-x}Ca_{0.2}Al_xFe_{12-2y}Pr_yMn_yO_{19}$

Dielectric Studies

The room temperature dielectric measurements were performed in 100Hz to 120MHz frequency range. Fig. 5a and 5b shows the variation of ε′ (dielectric constant) and ε′′ (dielectric loss factor) as a function of frequency for all the samples of $Ba_{0.8-x}Ca_{0.2}Al_xFe_{12-2y}Pr_yMn_yO_{19}$ *(x= 0.00, 0.04, 0.08 y= 0.00, 0.06, 0.09)*. It was observed that the ε′ (dielectric constant) decreases sharply with the rise in frequency at lower frequency up to intermediate frequency, and slightly rises at higher frequency. However, the ε′′ (dielectric loss) show the same behavior with ε′ at lower and intermediate frequency, whereas in higher frequency region it becomes almost independent of frequency. The high value observed at lower frequencies could be attributed to the presence of oxygen vacancies, interfacial dislocation, grain boundary defects, and the occurrence of large number of electrons hopping between Fe^{3+} and Fe^{2+}. Moreover, the slight increase in ε' at higher frequencies, will reduces the penetration depth of EM waves by increasing the skin effect. it can also be observed that sample MA2 has higher dielectric properties compared with MA1 and MA3.

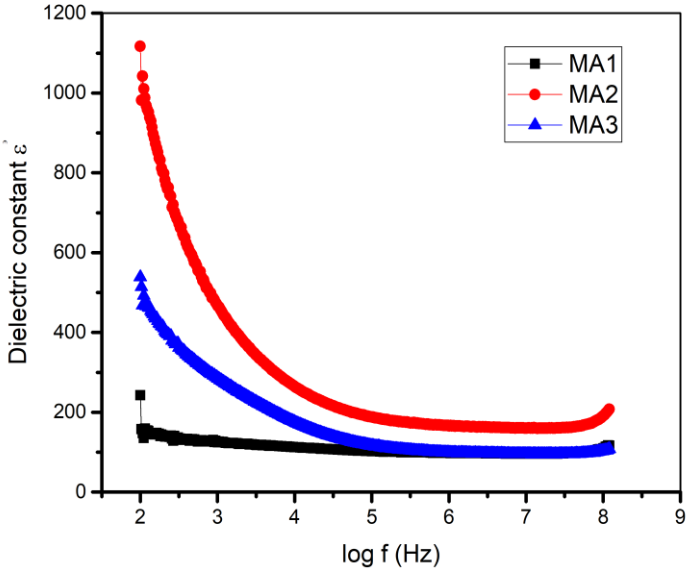

Fig. 5a: Variation of dielectric constant (ε′) with frequency for $Ba_{0.8-x}Ca_{0.2}Al_xFe_{12-2y}Pr_yMn_yO_{19}$ (x= 0.00, 0.04, 0.08 y= 0.00, 0.06, 0.09)

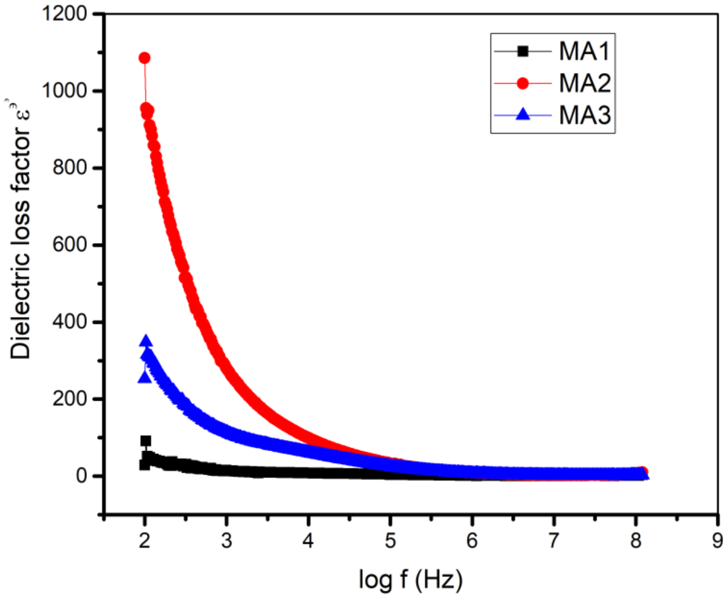

Fig. 5b: Variation of dielectric lost factor (ε′′) with frequency for $Ba_{0.8-x}Ca_{0.2}Al_xFe_{12-2y}Pr_yMn_yO_{19}$ (x= 0.00, 0.04, 0.08 y= 0.00, 0.06, 0.09)

Fig. 5c present the variation of dielectric loss factor/ tanδ as a function of frequency for all the samples of $Ba_{0.8-x}Ca_{0.2}Al_xFe_{12-2y}Pr_yMn_yO_{19}$ (x= 0.00, 0.04, 0.08 y= 0.00, 0.06, 0.09). Similar to the trend observed for ε′ with frequency, the tanδ values decreases with the increase in frequency at lower and intermediate frequency, and at higher frequencies it shows almost constant behavior because polarization is decreased at advanced fields. These variations seen with tanδ against the frequency can be ascribed to the phenomenon of conduction in ferrites, similar to the Koop's phenomenological theory. Lagging of polarization behind ac field dielectric loss arises and may be initiated by the impurities present, grain boundaries and crystal lattice imperfections. For sample MA3 a non-dependency on frequency was observed at intermediate frequency for some frequencies which later continue to decrease uniformly as the frequency increases. This deviation can be due to the change in resistance of sample with the concentration of the dopant substituted.

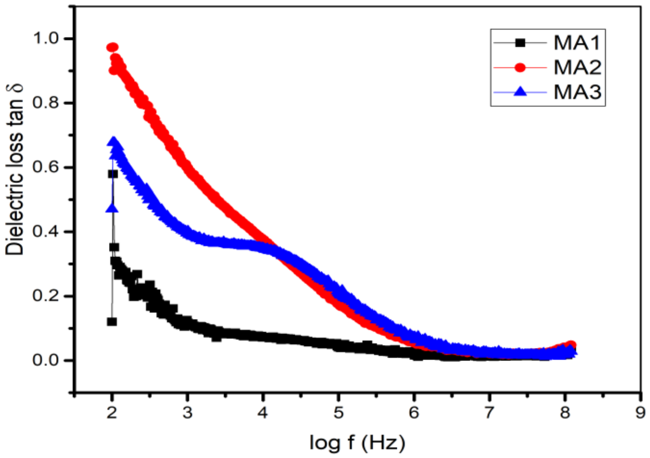

Fig. 5c: Variation of dielectric lost ($tan\delta$) with frequency for $Ba_{0.8-x}Ca_{0.2}Al_xFe_{12-2y}Pr_yMn_yO_{19}$ (x= 0.00, 0.04, 0.08 y= 0.00, 0.06, 0.09)

It was reported from various researchers that; a polycrystalline hexagonal ferrite sample is consist of grains (or parallel conducting plates) separated by grain boundaries (or resistive plates). These resistances contribute the dielectric and conducting behavior of the ferrite's material. In order to understand the nature and contributions of the grain and grain boundary resistance of the synthesized samples a Nyquist/cole-cole plots was used. This is a plot of the imaginary part (Z'') versus real part (Z') of complex impedance (Z^*) which consists of a semi-circle arc starting from the lower frequencies side to the higher frequencies side. The part of the semi-circle at the lower frequency side represents contribution of the grain boundaries (or grain boundary resistance (R_{gb}) while the part of the semi-circle at the higher frequency side of the Cole-Cole plot represents contribution from the grains (or grain resistance (R_g). Fig.5d presents the Cole-Cole plot of $Ba_{0.8-x}Ca_{0.2}Al_xFe_{12-2y}Pr_yMn_yO_{19}$ *(x= 0.00, 0.04, 0.08 y= 0.00, 0.06, 0.09)* at room temperature. It was observed that there is no higher frequency arc for all the substituted samples. Hence, we can conclude that there is no or less contribution from R_g towards the dielectric properties for these samples. The arc for the unsubstituted sample extends to higher frequency this indicates that the quantity of grains has increased and there is contribution from R_g towards the dielectric properties for this sample. With that, we can expect the substituted samples to be less conducting than the unsubstituted sample.

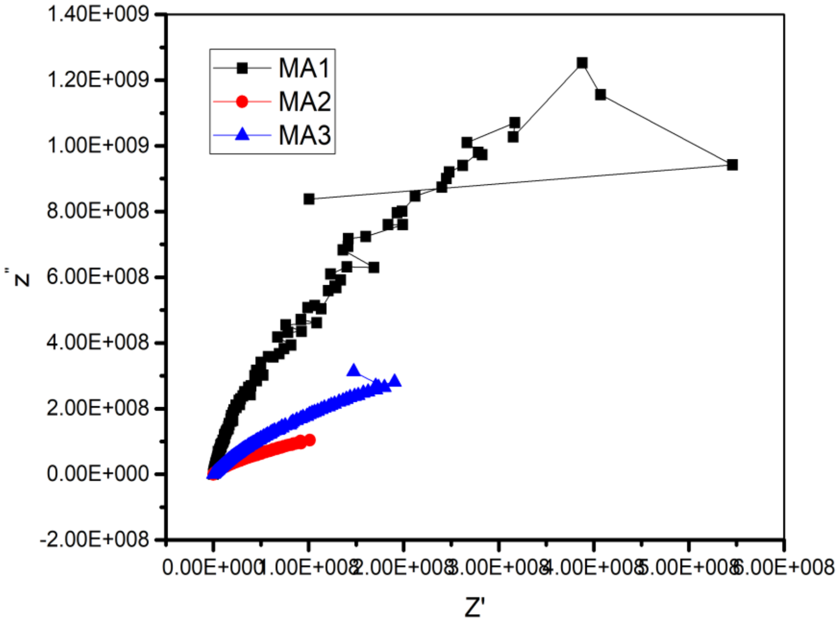

Fig. 5d: Cole-Cole plot of $Ba_{0.8-x}Ca_{0.2}Al_xFe_{12-2y}Pr_yMn_yO_{19}$ (x= 0.00, 0.04, 0.08 y= 0.00, 0.06, 0.09)

Fig. 5e shows the change of ac conductivity with frequency of $Ba_{0.8-x}Ca_{0.2}Al_xFe_{12-2y}Pr_yMn_yO_{19}$ *(x= 0.00, 0.04, 0.08 y= 0.00, 0.06, 0.09)* hexaferrite. It was observed from figure 5e that, the AC conductivity exhibits frequency independent behavior from lower to intermediate frequencies, but a sudden and abrupt rise in σ_{ac} of the prepared samples was observed in all the samples at higher frequency. This behavior is attributed to the fact that, at lower frequencies grain boundaries are more vigorous; therefore, the hopping frequency of electron among ferric (Fe^{3+}) and ferrous (Fe^{2+}) ion is small at lower frequencies. The conductive grains turn out to be more active as the frequency of applied field increases, thereby encouraging carriers hopping among two neighboring octahedral sites and a conversion between ferrous (Fe^{2+}) and ferric (Fe^{3+}) ions. Thus, conductivity linearly rises with frequency. Moreover, dispersion at high frequency is due to the conductivity of grains .

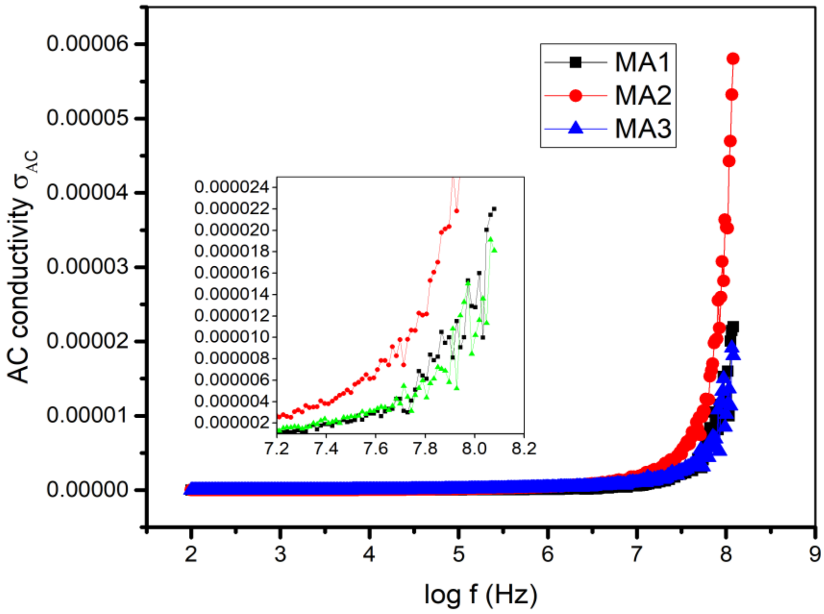

Fig. 5e: Variation of AC conductivity (σ_{ac}) with frequency for $Ba_{0.8-x}Ca_{0.2}Al_xFe_{12-2y}Pr_yMn_yO_{19}$ (x= 0.00, 0.04, 0.08 y= 0.00, 0.06, 0.09)

The variation of $ln\sigma_{ac}$ with $ln\omega$ for $Ba_{0.8-x}Ca_{0.2}Al_xFe_{12-2y}Pr_yMn_yO_{19}$ *(x= 0.00, 0.04, 0.08 y= 0.00, 0.06, 0.09)* is presented in fig. 5f. A linear relationship was observed between $ln\sigma_{ac}$ and $ln\omega$ with $ln\sigma_{ac}$ increasing steadily with increase in $ln\omega$, the slope of this linear graph gives the value of the exponent "s" in eqn. (1.0). It has been reported that the value of "s" usually lies between 0 and 1 and that when $s = 0$, the conduction mechanism is independent of frequency (i. e. DC conductivity) whereas it is dependent on frequency (i. e. ac conductivity) when $s \leq 1$. The slope of the linear plot of our sample (Fig. 5f) was found to be approximately 0.8, 0.6, and 0.6 for the samples MA1, MA2, and MA3 respectively. Hence, we can conclude ac conductivity to be the dominant conduction mechanism in the samples.

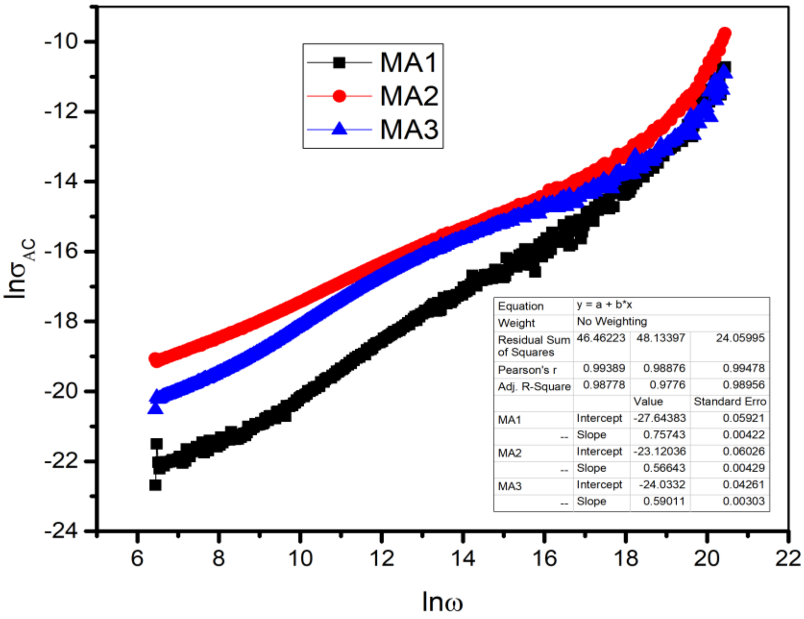

Equation	y = a + b*x		
Weight	No Weighting		
Residual Sum of Squares	46.46223	48.13397	24.05995
Pearson's r	0.99389	0.98876	0.99478
Adj. R-Square	0.98778	0.9776	0.98956
		Value	Standard Erro
MA1	Intercept	-27.64383	0.05921
--	Slope	0.75743	0.00422
MA2	Intercept	-23.12036	0.06026
--	Slope	0.56643	0.00429
MA3	Intercept	-24.0332	0.04261
--	Slope	0.59011	0.00303

Fig. 5f: Variation of $ln\sigma_{ac}$ with $ln\omega$ for *$Ba_{0.8-x}Ca_{0.2}Al_xFe_{12-2y}Pr_yMn_yO_{19}$* *(x= 0.00, 0.04, 0.08 y= 0.00, 0.06, 0.09)*

Complex modulus analysis of *$Ba_{0.8-x}Ca_{0.2}Al_xFe_{12-2y}Pr_yMn_yO_{19}$* *(x= 0.00, 0.04, 0.08 y= 0.00, 0.06, 0.09)* hexaferrites has been used to determine and inspect the dominating features of electrical transport mechanism such as ion hopping rate, conductivity relaxation time in the material. The variation of electric modulus (M′) and frequency is presented in Fig 5g. In was observed that M′ increase with continual increase frequency until it attains an extreme value/relaxation point and then decrease uniformly with increase in frequency.

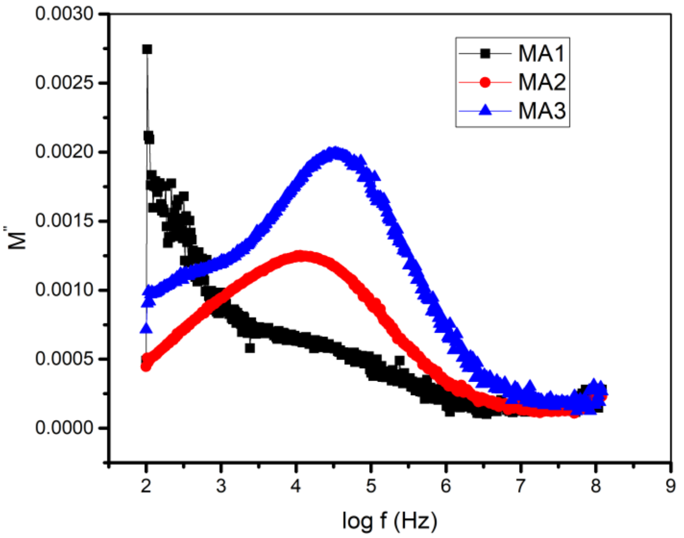

Fig. 5g: Variation of real part of electric modulus with frequency for *$Ba_{0.8-x}Ca_{0.2}Al_xFe_{12-2y}Pr_yMn_yO_{19}$* *(x= 0.00, 0.04, 0.08 y= 0.00, 0.06, 0.09)*

Table 3: Calculated electrical parameters from NOVA 1.1 sofware

SAMPLE CODE	Re	Rg	Cg	Rgb	Cgb	σ
MA1	63.9	3.22E+09	1.02pF	6.15E+06	3.31pF	2.20E-05
MA2	52.8	6.97E+06	1.96pF	1.4E+08	4.85pF	5.80E-05
MA3	81.9	2.77E+08	1.86pF	-1.28E+06	1.57pF	1.81E-05

Conclusıon

The synthesis of the substituted M-type hexagonal ferrites with $Ba_{0.8-x}Ca_{0.2}Al_xFe_{12-2y}Pr_yMn_yO_{19}$ *(x= 0.00, 0.04, 0.08 y= 0.00, 0.06, 0.09)* chemical composition was successful. The formation of pure single-phase hexagonal ferrites was confirmed from XRD analysis. There exists hematite in the doped samples whose cystallites sizes were in the range 20.5–26.33 nm. The lattice constants were found to decrease with increase in ions substitution. Dielectric constant was enhanced at high frequency in the entire sample and reduction of dielectric loss was also observed with further ions substitution. The grain boundary resistance contributes the most to the dielectric properties as revealed by the Nyquist plot, whereas the ac conductivity was the dominant conducting mechanism in the material and which was found to decrease with increase in ions substitution. Moreover, an improved particle size with better grain sizes better than those reported in literatures was obtained. Thus, an enhancement in the electrical properties is expected since smaller grains gave rise to improved dielectric properties resulting in decrese in energy loss.

References

Bhat, B. H., & Want, B. (2016). Magnetic, dielectric and complex impedance properties of lanthanum and magnesium substituted strontium hexaferrite. *Journal of Matterial Science, Material Electron,* 27, (12) 12582–12590.

Chawla, S. K., Kaur, P., Mudsainiyan, R. K., Meena,S. S., & Yusuf, S. M. (2015). Effect of fuel on the synthesis, structural, and magnetic properties of m-type hexagonal srfe12o19 nanoparticles. *J. Supercond. Nov. Magn.,* 28(5), 1589–1599.

Hafeez, H. Y., Tchouank Tekou, C. T., Mohammed, J., Bhat, B. H., Godara, S. K., & Srivastava, A. K. (2019). Structural, dielectric, and magneto-optical properties of al-cr substituted m-type barium hexaferrite. Phys. Status Solidi. 216(16), https://doi.org/10.1002/pssa.201800928

Mohammed, J., Suleiman, A. B., Hafeez, H. Y. Tchouank Tekou, C. T., Sharma, J. G., Bhadu, R., Sachin, K. G. & Srivastava, A. K. (2018). Effect of heat-treatment on the magnetic and optical properties of Sr0.7Al0.3Fe11.4Mn0.6O19. Mater. Res. Express, 5(8), 086106. https://doi.org/10.1088/2053-1591/aad1e5

Mohammed, J., Sharma, J., Tchouank Tekou C. T., & Srivastava, A. K. (2017). Effect of rare earth and transition element doping in bismuth multi-ferroic. AIP Conf. Proc., 1860, 020016 https://doi.org/10.1063/1.4990315

Mohammed, J., Tchouank Tekou, C. T., Hafeez, H., Basandrai, Y. D., Bhadu,G. R., Godara, S. K., Narang, S. B., & Srivastava, A. K. (2019). Electromagnetic interference (EMI) shielding, microwave absorption, and optical sensing properties of BaM/CCTO composites in K u –band. Results Phys. 13, 102307, https:doi.org/10.1016/j.rinp.2019.102307.

Mosleh, Z., Kameli, P., Poorbaferani, A., Ranjbar, M., & Salamati, H. (2016). Structural, magnetic and microwave absorption properties of Ce-doped barium hexaferrite, *J. Magn. Magn. Mater.,* 397, 101–107

Ndikilar, C. E., Mohammed, J., Hafeez, H. Y., Tchouank Tekou C. T., Sharma, J., Pradip K. M., Sachin, K. G., & Srivastava, A. K. (2019). Structural, dielectric, and magneto-optical properties of Cu^{2+}-Er^{3+} substituted nanocrystalline strontium hexaferrite. Mater. Res. Express, 6(5), 056111 https://doi.org/10.1088/2053-1591/ab063b

Pullar, R. C. (2012). Hexagonal ferrites: A review of the synthesis, properties and applications of hexaferrite ceramics. Prog. Mater. Sci. 57(7), 1191–1334.

Pullar, R. C., & Bhattacharya, A. K. (2001). The synthesis and characterization of the hexagonal Z ferrite, Sr3Co2Fe24O41, from a sol-gel precursor. Materials Research Bulletin. 36(78), 1531-1538.

Rafiq, M. A., Waqar, M., Mirza, T. A., Farooq, A., & Zulfiqar, A. (2017). Effect of Ni^{2+} substitution on the structural, magnetic, and dielectric properties of barium hexagonal ferrites (BaFe12O19). *Journal of Electronic Materials*, 46(1), 241-246.

Sharma, J., Mohammed, J., Kaur, R., Tchouank Tekou C.T., & Srivastava, A. K. (2017). Investigation of structural and magnetic properties of Ba0.3Gd0.7Co0.7Fe11.3O19 hexaferrite. AIP Conf. Proc., 1860, 20017 https://doi.org/10.1063/1.4990316

Sun, C., Sun, K., & Chui P. (2012). Microwave absorption properties of Ce-substituted M-type barium ferrite. *J. Magn. Magn. Mater.,* 324, 802–805

Tchouank Tekou, C. T., Mohammed, J., Basandrai, D., Bhadu, G.R., Kumar,S., Narang, S. B., & Srivastava, A. K. (2019). Design of nano-sized ¬ Pr3+–Co2+ substituted M-type strontium hexaferrites for optical sensing and electromagnetic interference (EMI) shielding in ¬ K u band. Appl. Phys. A. 125 (251), https:doi.org/10.1007/s00339-019-2545-5.

Tchouank Tekou C. T., Sharma, J., Mohammed, J., & Srivastava, A. K. (2017). Calcination temperature effect on the microstructure and dielectric properties of M-type strontium hexagonal ferritess. AIP Conf. Proc., 1860, 020007 https://doi.org/10.1063/1.4990306

Vadivelan, S., & Victor, J. N. (2016). Investigation of magnetic and structural properties of copper substituted barium ferrite powder particles via co-precipitation method. Results in physics 6, 843-850.